Available online at www.sciencedirect.com
SCIENCE DIRECT
Icarus 181 (2006) 408–418
ICARUS
www.elsevier.com/locate/icarus

Fresnel modeling of hematite crystal surfaces and application to martian hematite spherules

Timothy D. Glotch *, Philip R. Christensen, Thomas G. Sharp

Department of Geological Sciences, Arizona State University, Tempe, AZ 85287, USA

Received 13 September 2005; revised 4 November 2005

Available online 26 January 2006

Abstract

The gray crystalline hematite at Meridiani Planum first discovered by the Mars Global Surveyor Thermal Emission Spectrometer (MGS-TES) instrument occurs as spherules that have been interpreted as concretions. Analysis of the TES and mini-TES spectra shows that no 390 cm^{-1} feature is present in the characteristic martian hematite spectrum. Here, we incorporate the mid-IR optical constants of hematite into a simple Fresnel reflectance model to understand the effect of emission angle and crystal morphology on the presence or absence of the 390 cm^{-1} feature in an IR hematite spectrum. Based on the results we offer two models for the internal structure of the martian hematite spherules.

Keywords: Infrared observations; Mars, surface; Mineralogy; Spectroscopy

1. Introduction

The discovery of gray crystalline hematite at Meridiani Planum, Aram Chaos and Valles Marineris by the Mars Global Surveyor (MGS) Thermal Emission Spectrometer (TES) instrument (Christensen et al., 2000, 2001a, 2001b) was a major factor in the selection of the Meridiani Planum landing site for the Mars Exploration Rover (MER) Opportunity. Since the initial discovery of the martian hematite deposits, many hypotheses have been suggested for the hematite formation process. In general, the proposed hypotheses for martian hematite formation in Meridiani Planum fall into five categories: (1) aqueous deposition (Christensen et al., 2000, 2001a, 2001b; Glotch et al., 2004; Christensen and Ruff, 2004; Hynek, 2004), (2) oxidation of magnetite in ignimbrites or volcanic ash deposits (Noreen et al., 2000; Chapman and Tanaka, 2002; Hynek et al., 2002; Arvidson et al., 2003), (3) groundwater or hydrothermal deposition of hematite (Hynek et al., 2002; Catling and Moore, 2003; Chan et al., 2004; Ormö et al., 2004; McLennan et al., 2005), (4) fine-intimate hematite, possibly in the form of coatings (Kirkland et al., 2004), and (5) impact melt spherules (Burt et al., 2005; Chapman, 2005).

Much work has been done which shows that the infrared spectrum of hematite can vary with particle size, orientation, shape, and precursor mineralogy (Estep-Barnes, 1977; Rendon and Serna, 1981; Barron et al., 1984; Pecharromán and Iglesias, 2000; Lane et al., 2002; Glotch et al., 2004). Lane et al. (2002) showed that the thermal IR emissivity spectrum of the martian hematite as measured by TES has no absorption band at 390 cm^{-1}, as is seen in some terrestrial hematite spectra. This was confirmed by Glotch et al. (2004, 2005) who made use of factor analysis and target transformation techniques (Malinowski, 1991; Bandfield et al., 2000, 2002) to analyze the TES and mini-TES data sets (Fig. 1). Lane et al. (2002) interpreted the lack of a 390 cm^{-1} feature as evidence for (001) face (**c**-face) dominated emission, which occurs if hematite crystals are platy (Lane et al., 2002) or acicular (Glotch et al., 2004). Because formation processes can determine the shape of the hematite crystals, the presence or absence of the 390 cm^{-1} band can lend some insight into the origin of the hematite.

In this work, we make use of dielectric dispersion theory (Lorentz, 1880; Lorenz, 1881) to model the optical constants of hematite from laboratory thermal emission spectra. The derived

* Corresponding author. Now at Division of Geological and Planetary Sciences, California Institute of Technology, M.C. 150-21, Pasadena, CA 91125, USA. Fax: +1 (626) 585 1917.
E-mail address: tglotch@gps.caltech.edu (T.D. Glotch).

0019-1035/$ – see front matter
doi:10.1016/j.icarus.2005.11.020

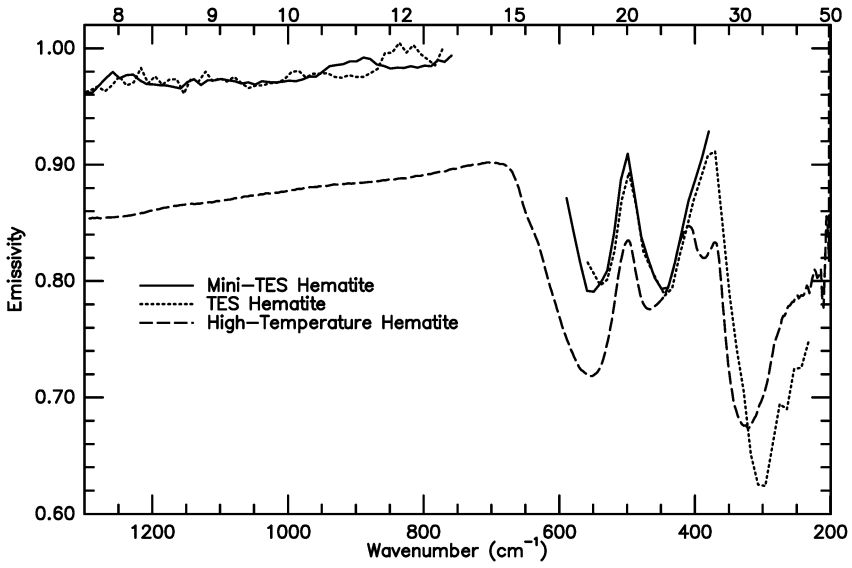

Fig. 1. The martian hematite spectrum derived from mini-TES and TES exhibits no 390 cm^{-1} feature. In contrast, a spectrum of a natural volcanic hematite from Durango, Mexico has a feature at 390 cm^{-1}.

optical constants are then inserted into the Fresnel equations to determine the necessary conditions for the presence or absence of the 390 cm^{-1} absorption band in the infrared emission spectrum of hematite. Specifically, we examine the effects of crystal morphology and emission angle from hematite crystal surfaces.

Previously, the optical constants of hematite from 30 to 1000 cm^{-1} had been determined using dispersion theory by Onari et al. (1977) from reflectance measurements. It is unclear, however, if a single crystal (the ideal case) was used to determine the reflectance spectra and optical constants. Here we use measurements of emissivity of the ordinary and extraordinary (O and E) rays of a single hematite crystal to determine the optical constants. We extend the range of the optical constants to 1500 cm^{-1}, although our measurements are terminated at 200 cm^{-1}. The optical constants, however, do cover the full range measured by the TES and mini-TES (Christensen et al., 2001a, 2001b, 2003) instruments. The use of dispersion theory to calculate the optical constants of a mineral from its emissivity spectrum has been demonstrated by Wenrich and Christensen (1996) and Lane (1999).

2. Dispersion theory and Fresnel modeling

Dispersion theory is a mathematical formulation that represents the vibration of a crystal lattice as the sum of the vibrations of two or more harmonic oscillators. The vibration of each oscillator creates a moving dipole moment, which in turn produces the radiation that is measured in an infrared spectrum. Each oscillator is defined by three parameters: ν, $4\pi\rho$, and γ, which represent the center frequency of the oscillation, the band strength, and damping coefficient, respectively. An additional term, ε_0, is the high frequency dielectric constant, which is a bulk mineral property rather than an oscillator-dependent property. Dispersion equations vary slightly in the literature, but we adopt the formulation of Spitzer and Kleinman (1961), which is widely used. As described by Spitzer and Kleinman (1961), dispersion theory relates these properties of the oscillators in a mineral to the optical constants, n and k by the following equations:

$$n^2 - k^2 = \varepsilon_0 + \sum_j \frac{4\pi\rho_j \nu_j^2(\nu_j^2 - \nu^2)}{(\nu_j^2 - \nu^2)^2 + (\gamma_j^2 \nu_j^2 \nu^2)}, \tag{1}$$

$$nk = \sum_j \frac{2\pi\rho_j \nu_j^2(\gamma_j \nu_j \nu)}{(\nu_j^2 - \nu^2)^2 + (\gamma_j^2 \nu_j^2 \nu^2)}, \tag{2}$$

where n is the real index of refraction, k is the imaginary index of refraction, and j represents the jth oscillator. Light that interacts with crystals is polarized into ordinary (O) and extraordinary (E) rays. In hexagonal, uniaxial minerals such as hematite, the E ray propagates perpendicular to the c axis, and the O ray propagates both parallel and perpendicular to the c axis. The derived values for the optical constants for the O and E rays may be inserted into the simplified Fresnel equation to calculate reflectivity as a function of wavelength for specular surfaces.

$$R_T = \frac{R_\perp^2 + R_{||}^2}{2}, \tag{3}$$

where

$$R_{||}^2 = \frac{(\cos\theta - u)^2 + \nu^2}{(\cos\theta + u)^2 + \nu^2}, \tag{4}$$

$$R_\perp^2 = \frac{[(n^2 - k^2)\cos\theta - u]^2 + (2nk\cos\theta - \nu)^2}{[(n^2 - k^2)\cos\theta + u]^2 + (2nk\cos\theta + \nu)^2}, \tag{5}$$

$$u = \left(\frac{n^2 - k^2 - \sin^2\theta + [(n^2 - k^2 - \sin^2\theta)^2 + 4n^2k^2]^{1/2}}{2}\right)^{1/2}, \tag{6}$$

$$\nu = \left(\frac{-(n^2 - k^2 - \sin^2\theta) + [(n^2 - k^2 - \sin^2\theta)^2 + 4n^2k^2]^{1/2}}{2}\right)^{1/2}, \tag{7}$$

and θ is the angle of incident radiation measured from the surface normal. $R_\perp$ and $R_\parallel$ are amplitudes and must be squared to get the fractional intensities, which are the measured parameters (Born and Wolf, 1980).

When $\theta = 0$, the Fresnel equation simplifies to

$$R = \frac{(n-1)^2 + k^2}{(n+1)^2 + k^2}. \tag{8}$$

Reflectivity is then converted to emissivity according to Kirchoff's Law:

$$\varepsilon = 1 - R - T. \tag{9}$$

For a thick sample, T, the transmittance is equal to zero, so emissivity is simply $1 - R$.

Dispersion analysis is performed by iteratively adjusting the oscillator parameters until the best possible fit (minimum root mean square error) is achieved between the modeled spectrum and the spectrum measured in the laboratory. A successful dispersion analysis meets the following requirements: (1) the measured and modeled spectra agree within reasonable estimates of the experimental error, (2) the number of oscillators used in the analysis is the minimum that the data require, and (3) the dispersion parameters are uniquely determined by fitting the modeled spectrum to the measured (Spitzer and Kleinman, 1961).

3. Methods

3.1. Instrumentation

Thermal infrared (200–2000 cm^{-1}) emission spectra were collected at 2 cm^{-1} sampling (4 cm^{-1} spectral resolution) on Arizona State University's Nicolet Nexus 670 E.S.P. Fourier-Transform Infrared (FTIR) spectrometer modified to collect polarized emission spectra. Each sample spectrum is an average of 500 scans collected while the sample was maintained at 80 °C. Details of the collection procedure, laboratory setup and calibration process can be found in Christensen and Harrison (1993) and Ruff et al. (1997). The polarizer used in this study is a KRS-5 gold wire grid polarizer manufactured by Pike Technologies with a spectral range of 20,000 to 250 cm^{-1}. Polarization angle accuracy is ±2.5°.

3.2. Sample

The hematite sample used in this study is a platy hematite crystal from Brumado, Bahia, Brazil with a diameter of 2.4 cm and a thickness of 3 mm. The small thickness of the crystal posed a problem in measuring the emissivity of the (100) face, so the crystal was cut into three pieces perpendicular to the (001) face (**c**-face) and perpendicular the [100] axis. The three pieces were then bound together with epoxy so that the result was a crystallographic (100) face with an effective diameter of 0.9 cm. The final 0.9-cm sample was polished to optical smoothness, ensuring specular reflection at infrared wavelengths.

4. Results and discussion

4.1. The emissivity spectra of hematite

Neither the O ray nor the E ray of hematite measured in this study exhibits a feature at 390 cm^{-1} (Fig. 2). Rather, we find that it is certain combinations of these rays that lead to the presence of the 390 cm^{-1} feature in some hematite spectra. The hematite ordinary ray spectrum has three broad absorption bands centered at 319, 456, and 560 cm^{-1} in the spectral range 200–2000 cm^{-1}. The extraordinary ray has two bands centered at 314 and 558 cm^{-1}. Onari et al. (1977) report a fourth band belonging to the ordinary ray at 227 cm^{-1}. The CsI beamsplitter in the spectrometer used to acquire spectra for this study has a sharp dropoff in throughput in this region, preventing reliable detection of the 227 cm^{-1} band. The O and E ray spectra are shown in Fig. 2. The O ray spectrum was acquired directly by measuring the (001) face of a hematite crystal and the E ray spectrum was acquired by measuring the (100) face through a polarizing filter which removed O ray energy from the spectrum.

4.2. Dispersion analysis and derivation of optical constants

Hematite has the same hexagonal crystal structure as corundum. Factor group analysis of the normal modes of the corundum crystal structure (Bhagavantam and Venkatarayuku, 1939) yields the matrix irreducible representations:

$$\Gamma = 2A_{1g} + 2A_{1u} + 3A_{2g} + 3A_{2u} + 5E_g + 5E_u, \tag{10}$$

where Γ is just the sum of irreducible representations, A stands for 1-dimensional irreducible representations, and E stands for 2-dimensional irreducible representations. The subscripts u and g are details of the symmetry operations related to the point groups described by the irreducible representations.

Of these modes, the two one-dimensional A_{2u} and four two-dimensional E_u modes are infrared active, whereas the other modes are Raman active. A symmetry analysis (Cowley, 1969) showed that the E_u modes correspond to the O ray and the A_{2u} modes correspond to the E ray. Because hematite shares the crystal structure of corundum, the same is true for the hematite crystal structure, as shown by Rendon and Serna (1981). The symmetry analysis limits the number of oscillators that can be used in modeling the O and E rays of hematite. Modeling more than four oscillators for the O ray or more than two oscillators for the E ray would be physically meaningless, so the number of oscillators used in a dispersion analysis is constrained by the symmetry.

The emissivity spectra of the O and E rays of hematite acquired for this study were modeled using a dispersion analysis. Dispersion parameters for each oscillator were adjusted until the lowest root mean square (RMS) emissivity error between the measured and modeled spectra was achieved. Comparison of the measured and modeled spectra (Fig. 3) shows good agreement, with RMS emissivity errors of 0.049 and 0.062% for the O and E rays, respectively.

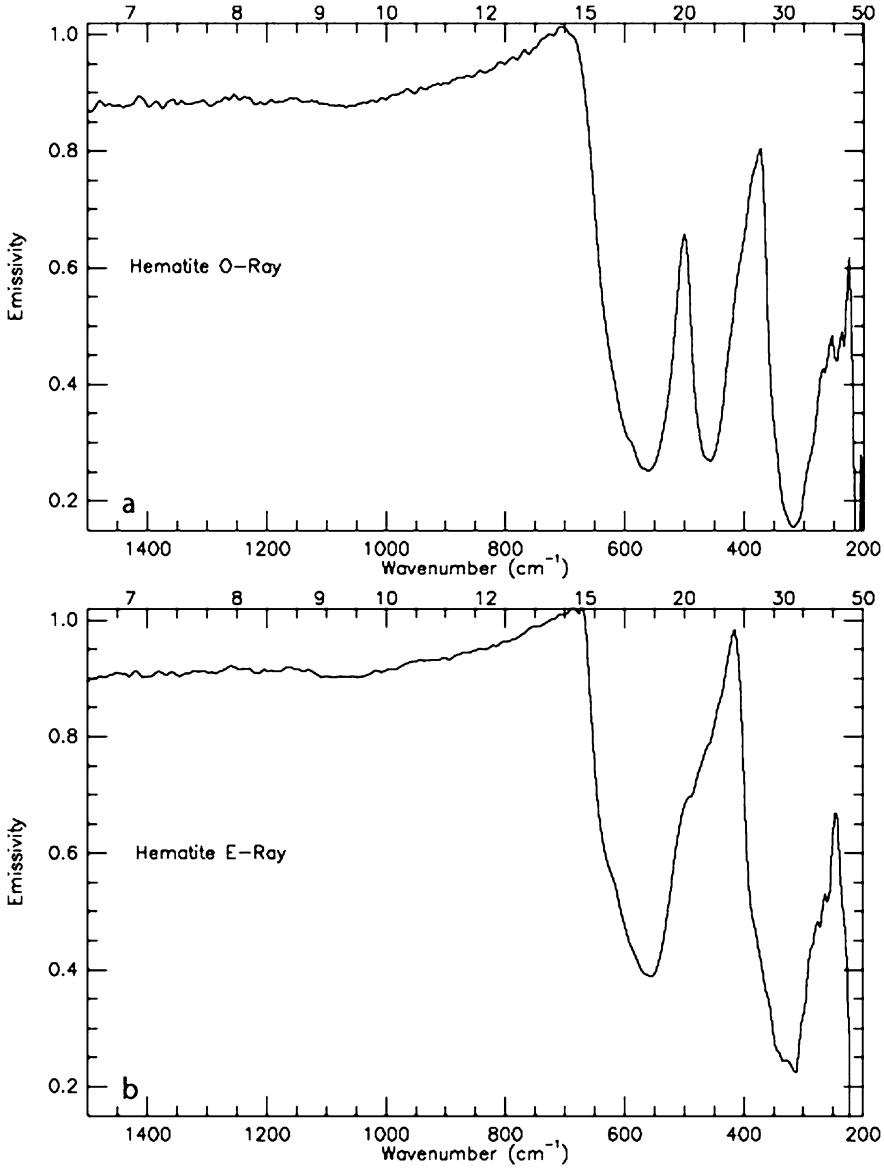

Fig. 2. Measured spectra of a single hematite crystal. (a) Hematite ordinary ray. (b) Hematite extraordinary ray.

The dispersion oscillator parameters used to produce the modeled spectra in Fig. 3 are listed in Table 1, and the values of n and k derived from the oscillator parameters, compared to the values of Onari et al. (1977) are shown in Figs. 4 and 5. The optical constants presented here can be found at http://www.gps.caltech.edu/~tglotch/optical_constants.htm or by contacting the primary author. In Table 1, the values derived by Onari et al. (1977) for each parameter are listed next to the values derived in this study. In the case of the damping term (γ), the second value listed is converted from the original reported by Onari et al. (1977), and the third value is their original reported value. As noted earlier, the dispersion equations vary slightly in the literature, and Onari et al. (1977) use a slightly different formulation than that used by Spitzer and Kleinman (1961), Wenrich and Christensen (1996), and Lane (1999). This alternate formulation affects only the values of the damping term (γ). To directly compare the work presented here to that of Onari et al. (1977), their γ values were converted according to the following relationship:

$$\gamma = \gamma_j / \nu_j, \tag{11}$$

where γ is the value reported in this study, γ_j is the damping term value from Onari et al. (1977) for the jth oscillator, and ν_j is the center position of the jth oscillator in wavenumbers.

The values of the dispersion parameters differ because the spectra acquired by Onari et al. (1977) and those for this study are not identical. The measured spectra determine the modeled dispersion parameters and optical constants, so this result is not surprising. Inspection of the modeled spectra from this study and Onari et al. (1977) (Fig. 6) shows some small differences between the spectra.

In modeling the O-ray emissivity spectrum of hematite, the low signal at long wavelengths made it difficult to model the absorption due to the longest wavelength oscillator (Table 1) at 216 cm^{-1}. The modeled center frequency for this oscillator

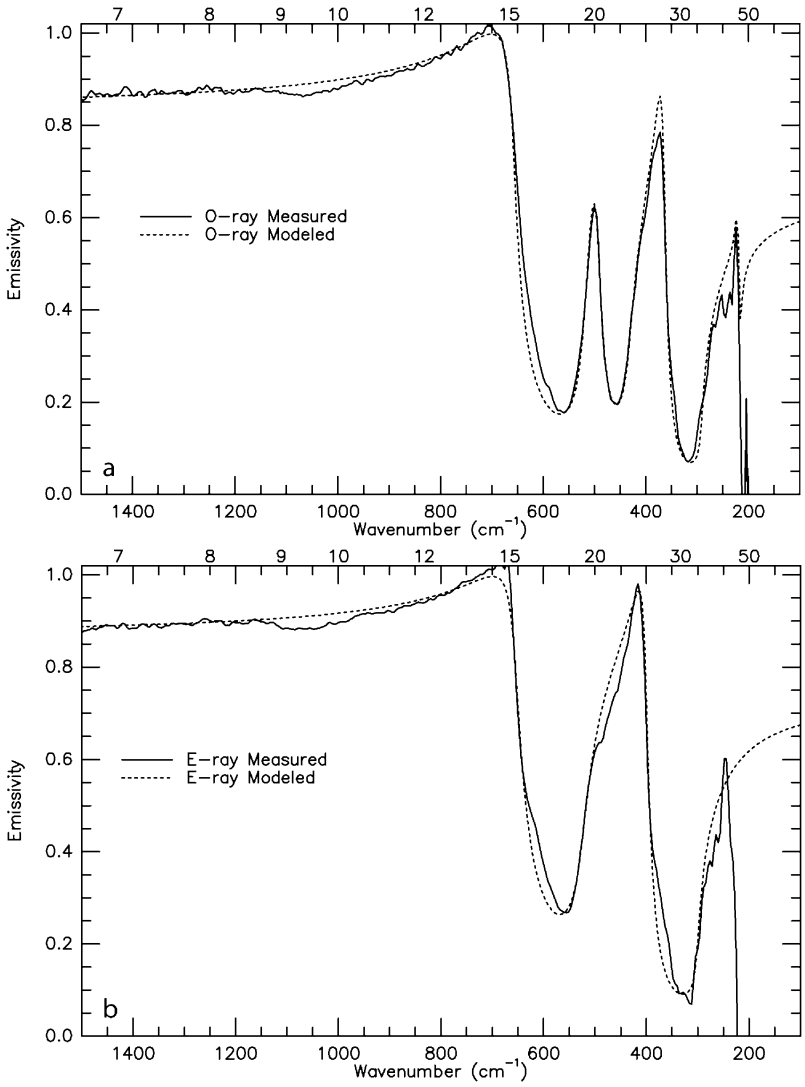

Fig. 3. Measured hematite spectra compared with spectra modeled using dispersion theory. (a) Measured and modeled ordinary ray. Spectral RMS is 0.049. (b) Measured and modeled extraordinary ray. Spectral RMS is 0.062.

differs substantially from that obtained by Onari et al. (1977). Nevertheless, use of the exact dispersion parameters of Onari et al. (1977) for this oscillator results in a poorer model fit over the entire wavelength range of the hematite spectrum. The values of ε_0 derived here for both the O and the E rays are also different from those of Onari et al. (1977). The main cause of this is the higher overall emissivity of our spectra from ∼700 to 1500 cm^{-1} (Fig. 6).

4.3. Spectral variation in hematite due to emission angle and crystal morphology

From the dimensions of the hematite crystal used in this study, it is possible to approximate the relative contributions of emissivity from the [001] axis (O ray) and all axes perpendicular to it (O ray + E ray). Approximating a hematite crystal as a disk with a radius of 24 mm and a height of 3 mm, the area of the (001) face is 1810 mm^2, and the combined area of the side (edge) of the disk is 452 mm^2. The side of the disk (all faces perpendicular to (001)) makes up 25% of the total area and is therefore responsible for 25% of the observed emissivity. This simple model assumes that the (001) faces and all faces perpendicular to them are always contributing the same amount of emissivity to the spectrum. The following discus-

Table 1
Oscillator parameters for the ordinary and extraordinary rays of hematite

ν (cm^{-1})	$4\pi\rho$	γ	E_0
	Ordinary ray		
216 (227)[a]	1.10 (1.1)	0.025 (0.018; 4)	
292 (286)	9.00 (12.0)	0.028 (0.028; 8)	5.5 (7.0)
433 (437)	2.70 (2.9)	0.050 (0.046; 20)	
517 (524)	0.68 (1.1)	0.050 (0.048; 25)	
	Extraordinary ray		
301 (299)	6.50 (11.5)	0.035 (0.050; 15)	4.5 (6.7)
525 (526)	1.54 (2.2)	0.057 (0.057; 30)	

[a] The values in parentheses are those reported by Onari et al. (1977). For the values of γ in parentheses, the first number represents the Onari et al. value converted to the system described here. The second value is that originally reported by Onari et al.

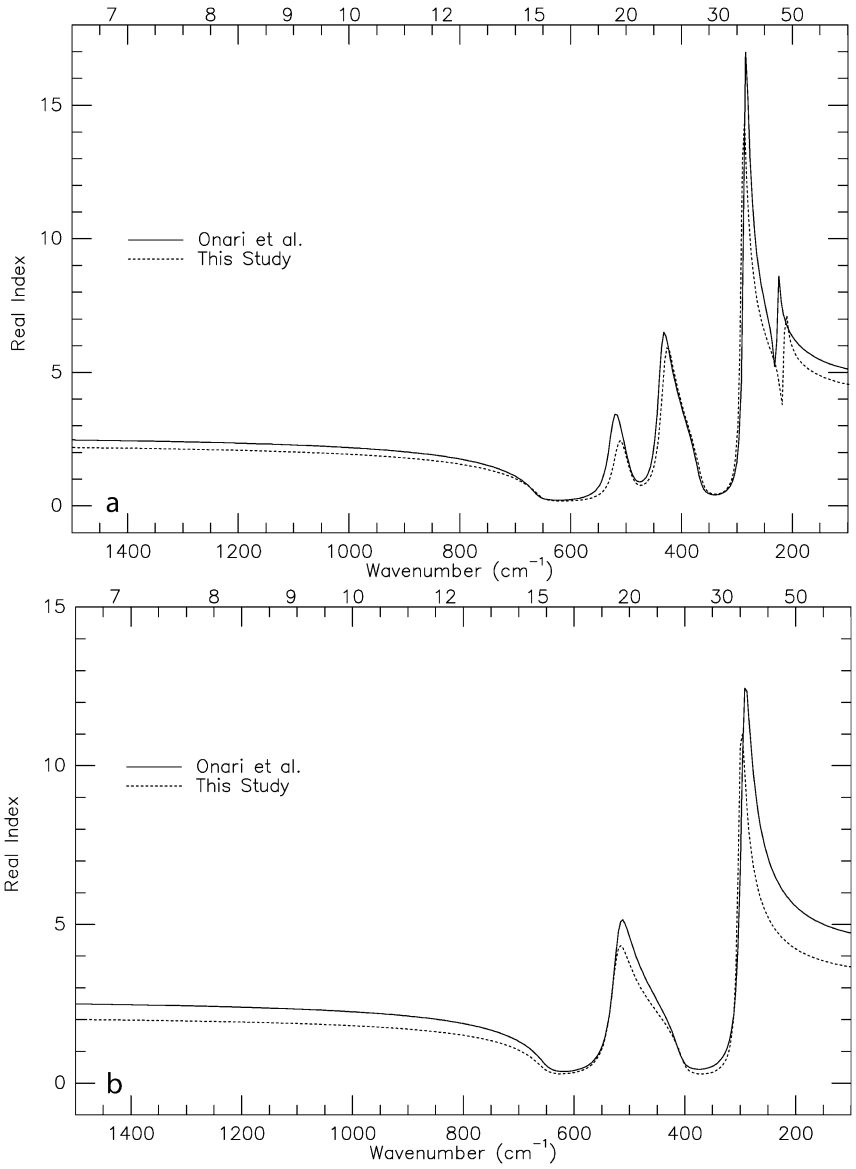

Fig. 4. Modeled wavelength-dependent real index of refraction (n) from this study and Onari et al. (1977). (a) Ordinary ray. (b) Extraordinary ray.

sion assumes specular hematite crystal surfaces with varying amounts of [001] and [100] emissivity, as would be the hypothetical case for a spherule of hematite composed of randomly oriented platy hematite particles of varying thicknesses (Fig. 7). The total amount of [001] and [100] emissivity observed from the surface would be controlled by the thickness of the platy hematite crystals, as thicker crystals would increase the amount of non-[001] emissivity. The goal of this simple model is not to accurately reproduce the spectral shape of each band in the hematite emissivity spectrum, but rather to determine the conditions necessary for the presence or the absence of the 390 cm^{-1} feature. Bell et al. (2004) reported the presence of specular glints originating from the spherules in Pancam images. This indicates that the spherules are smooth at visible wavelengths. Therefore, the spherules must also be smooth at infrared wavelengths, and more complicated reflectance or emission models (e.g., Vincent and Hunt, 1968; Hunt and Vincent, 1968; Conel, 1969; Hapke, 1981, 1984, 1986, 1993; Moersch and Christensen, 1994) are not needed to accurately predict the presence or absence of this band.

To model the spectrum of a specular hematite spherule comprised of randomly oriented micro-crystals, we make use of a variation of Eq. (1), which assumes equal contributions from the O and E rays as well as equal emission angles for each ray. This is not the case for a platy or lathy hematite crystal which is dominated by [001] emission of the O ray. Emission along the [001] axis of hematite is composed entirely of the O ray, while emission along the [100] axis and all axes perpendicular to the [001] axis is composed of equal parts O ray and E ray. Additionally, the model of a platy hematite crystal calls for a large percentage of the emissivity along the [001] axis, and a simple average, as in the case of Eq. (1) is not in order. Finally, the [001] and [100] axes are perpendicular to each other, so when calculating the total emissivity, if the emission angle from the [001] axis is θ, then the emission angle from the [100] and all faces perpendicular to [001] will be $90 - \theta$.

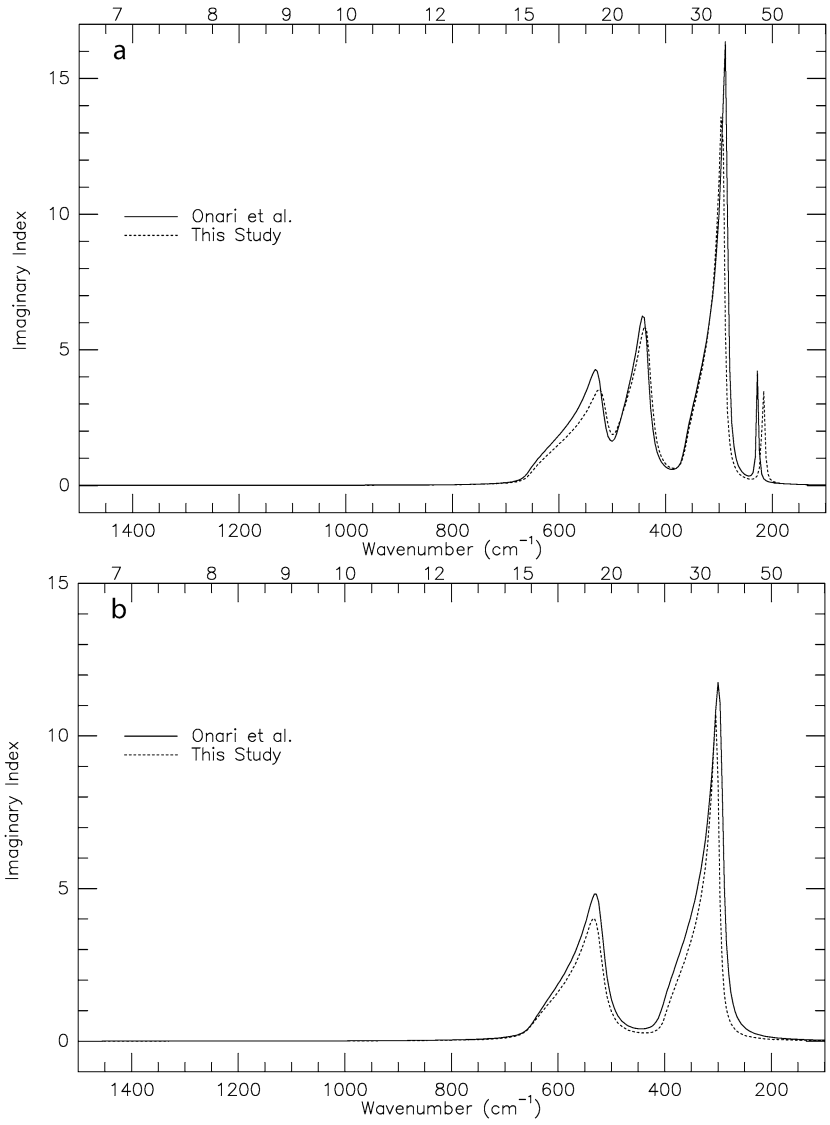

Fig. 5. Modeled wavelength-dependent imaginary index of refraction (k) from this study and Onari et al. (1977). (a) Ordinary ray. (b) Extraordinary ray.

For the case of a hematite surface that has 75% of the emission coming from the (001) face (Fig. 8), the equation for total specular reflectance will be

$$R_T = 0.75R^2_{(001)} + 0.25R^2_{(100)}, \tag{12}$$

where $R^2_{(001)} = R^2_{\perp}$, as in Eq. (3), and

$$R^2_{(100)} = \left(\frac{R_{\perp} + R_{||}}{2}\right)^2 \tag{13}$$

and θ in Eqs. (2) and (3) is replaced by $90 - \theta$. Reflectance is converted to emissivity via Eq. (9).

At emission angles from 0° to 45°, the spectra in Fig. 8 are similar to each other, with an overall increase in emissivity as the emission angle increases. A kink in each spectrum is present at ~400 cm^{-1}, which becomes more pronounced as the emission angle increases. This kink appears to be a precursor for the full 390 cm^{-1} feature which appears under different conditions. At an emission angle of 60°, the kink at 400 cm^{-1} is most pronounced, but is still not a fully developed 390 cm^{-1} feature. Additionally, the 560 cm^{-1} band shifts to shorter wavelengths. At an emission angle of 75°, all spectral features are shifted to shorter wavelengths, and there is a small kink at 400 cm^{-1}, but unlike the spectra at lower emission angles, the kink is present on the low wavenumber side of the local emissivity maximum.

The hematite sample measured for this study is thick compared to most naturally occurring platy hematite crystals. For a modeled hematite surface composed of plates with an even higher proportion of [001] axis emission (thinner crystal), a 390 cm^{-1} feature does not appear at any emission angle (Fig. 9a). This result is supported by spectra acquired of natural schistose hematite samples (composed of thin plates), which showed no 390 cm^{-1} feature at angles as high as 45° (Lane et al., 2002). For the 90% [001] emission (Fig. 9a), there is no 390 cm^{-1} feature, although a slight 400 cm^{-1} kink is observable at the 45° and 60° emission angles. For modeled hematite surfaces composed of crystals of greater thickness, a smaller proportion of the total emissivity is from the [001] axis. Models of hematite crystals with 60% [001] emissivity show that both the decreas-

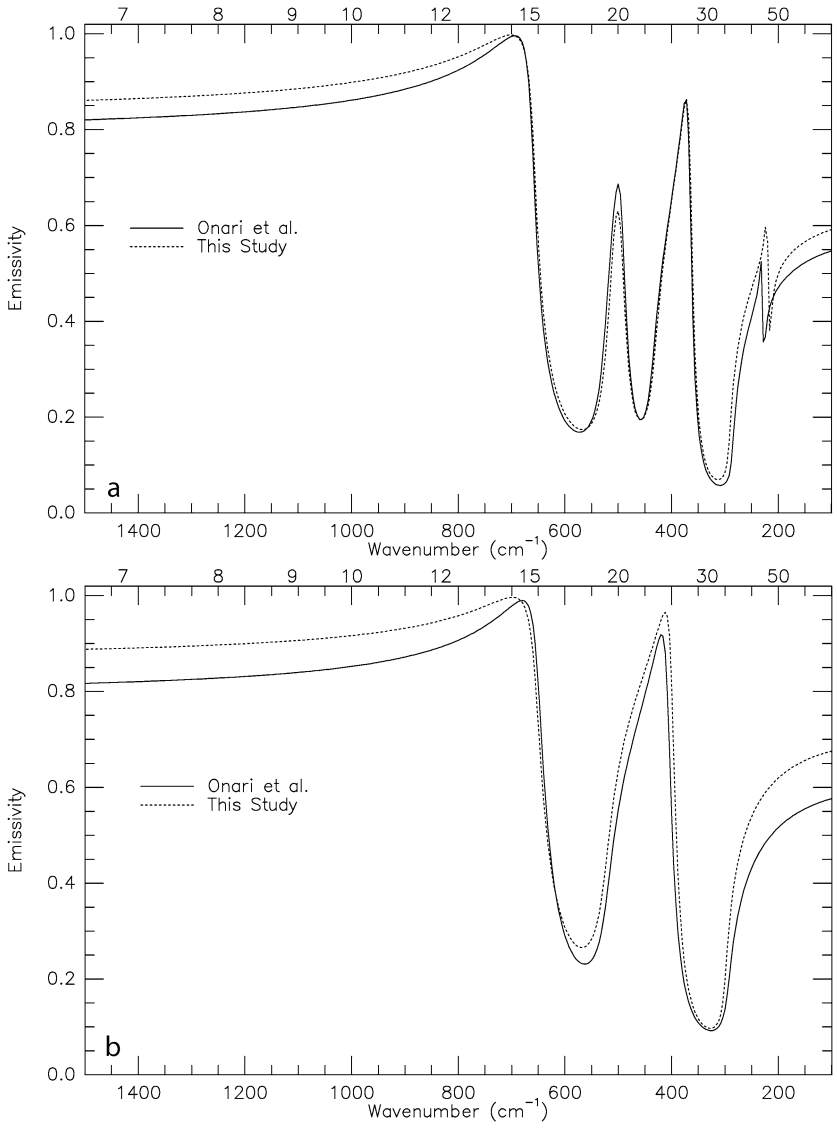

Fig. 6. Modeled hematite emissivity spectra from this study and Onari et al. (1977). (a) Ordinary ray. (b) Extraordinary ray.

ing proportion of [001] axis emission and increasing emission angle cause the presence of the 390 cm^{-1} feature (Fig. 9b). With the 90% [001] axis contribution, a fully developed 390 cm^{-1} feature is never apparent. Conversely, in the case of 60% [001] emission, a small 390 cm^{-1} feature is present at a 15° emission angle, and the 390 cm^{-1} feature is fully developed at a 30° emission angle.

5. Application to Mars

The theoretical spectra presented above show that when thermal emission spectra are collected of hematite surfaces dominated by [001] axis emission, there should not be a fully developed 390 cm^{-1} feature, even at angles as high as 75° relative to the (001) face (Figs. 8 and 9a). This is due to the fact that a combination of O- and E-ray emission is needed to see the 390 cm^{-1} feature in the infrared emissivity spectrum, and emissivity along the [001] axis is composed entirely of O-ray emissivity.

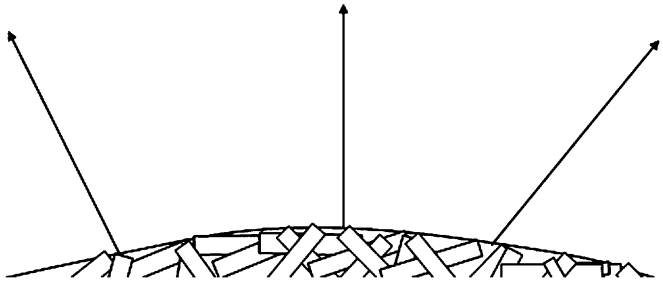

Fig. 7. Schematic of a specular hematite surface composed of randomly oriented hematite plates. The total [001] and [100] emission from the surface depends on the thickness of the hematite plates.

These results have some implications for observations of the hematite-rich spherules seen at Meridiani Planum. Because TES and mini-TES observations of the martian hematite show no 390 cm^{-1} feature in the hematite spectra (Lane et al., 2002; Glotch et al., 2004, 2005), the spectra of the spherules must be dominated by [001] axis emission. Two models for how this

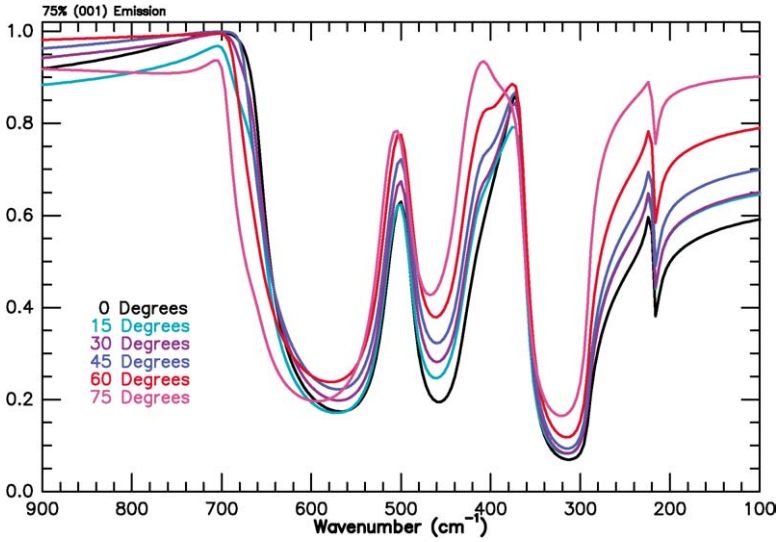

Fig. 8. Modeled emissivity spectra of a specular hematite surface with 75% of the total emission due to the hematite (001) face. Although no fully developed 390 cm^{-1} feature is present, a prominent kink near 400 cm^{-1} is seen at higher emission angles.

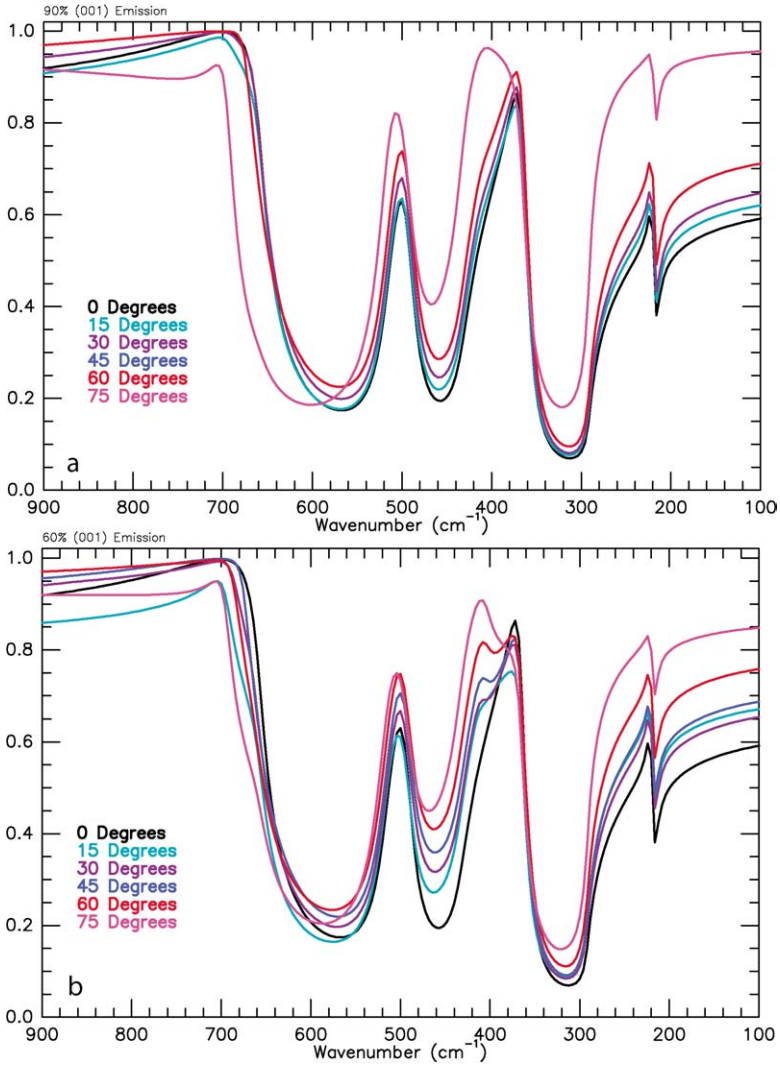

Fig. 9. Modeled emissivity spectra of specular hematite surfaces. (a) 90% of total emission due to the hematite (001) face. No 390 cm^{-1} feature is seen, although a 400 cm^{-1} kink is seen at 45° and 60° emission angles. (b) 60% of the total emission due to the hematite (001) face. A fully developed 390 cm^{-1} feature is present at 45° and 60° emission angles, and kinks are present at 15° and 30° emission angles.

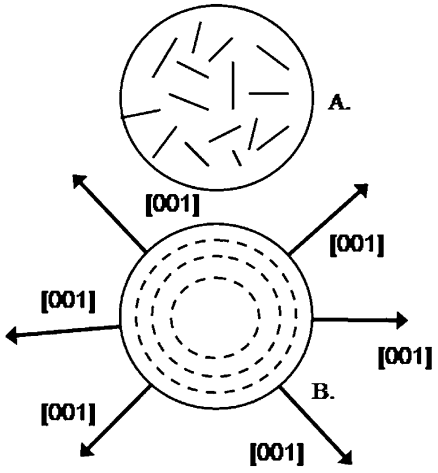

Fig. 10. Two models for the internal structure of the martian hematite-rich spherules. Model A depicts the spherule composed of randomly oriented individual euhedral platy hematite crystals. Model B depicts the spherule composed of concentrically grown anhedral hematite crystals with a lattice preferred orientation that causes the spherule to be dominated by [001] axis emission at any orientation.

might occur are illustrated in Fig. 10. Model A is a hematite spherule that is composed of randomly oriented platy hematite crystals, as discussed above. Because the infrared spectrum of platy hematite does not have a 390 cm^{-1} feature, even at high emission angles, the spectrum of randomly oriented hematite plates arranged in a spherical mass would also lack a 390 cm^{-1} feature.

Model B is a hematite spherule with no euhedral platy hematite crystals. If the hematite spherules are concretions, then their formation does not require the formation of individual euhedral crystals. Instead, the crystals may grow and form an anhedral mass with a radiating lattice-preferred orientation. If the concretions grew concentrically with [001] oriented radially, then their infrared spectra would be composed of [001] dominated emission in all directions. Although there are no individual crystal plates to measure, the spherule surfaces are specular, so the general Fresnel equation still applies. These two models are not the only possible models for the internal structure of the hematite spherules, but any proposed model must take into account the [001] dominated emission as viewed by the TES and mini-TES instruments.

The dominant [001] emission of the martian spherules does make certain hematite formation mechanisms less likely. Glotch et al. (2004) have shown that infrared spectra of hematite samples derived at high temperatures in the laboratory (500–700 °C) are poor matches to the martian hematite spectrum in terms of band shape, position, and the presence of the 390 cm^{-1} band. A major reason for the mismatch is the lack of [001] dominated emission in these samples. So, hematite formation processes that occur at high temperatures, or preferentially create hematite crystals with roughly equal amounts of [001] and other rays are less likely to be responsible for the martian hematite spherules. These processes include the formation of impact-melt spherules (Chapman, 2005; Burt et al., 2005) at high temperature, or the high-temperature oxidation of volcanic lapilli (Knauth et al., 2005).

6. Conclusions

Platy hematite crystals with a large percentage (90%) of [001] axis emission display no 390 cm^{-1} feature, even at high emission angles relative to the (001) face. For increasingly thick plates, a prominent kink at 400 cm^{-1}, and then a fully developed 390 cm^{-1} feature forms. When the percentage of emission from the faces perpendicular to (001) starts to approach that of (001) face emission, the 390 cm^{-1} feature is easily formed even at a relatively low emission angle of 30°.

Images from the MER Opportunity have shown that the martian hematite, at least at Meridiani Planum, occurs as ∼3–5-mm spherules that have been interpreted as concretions (Squyers et al., 2004; Herkenhoff et al., 2004; Chan et al., 2004). Observations of the hematite spectrum from orbit and the surface (Lane et al., 2002; Glotch et al., 2004) have shown that no 390 cm^{-1} feature is present in the thermal infrared spectrum. This observation can be explained if the spherules are (1) composed of randomly oriented thin plates or laths that are ∼90% or more (001) face by area, or (2) composed of crystals that have grown concentrically with a radial [001] lattice preferred orientation.

Given the [001] dominated emission of the spherules, it is likely that they formed at low temperature, thus ruling out such formation mechanisms as impact melt spherules, volcanic lapilli, or other mechanisms that do not create hematite dominated by [001] emission.

Acknowledgments

The authors thank Melissa Lane and Bruce Hapke for constructive comments that enhanced the content and clarity of the manuscript. We also thank Joshua Bandfield, Deanne Rogers, and Robin Fergason for reviews and discussion regarding an early version of the manuscript. We also thank Kelly Bender, Kim Murray, Kim Homan, Noel Gorelick, Sadaat Anwar, and Greg Mehall at Arizona State University for their planning, acquisition, processing, and software support of the TES and mini-TES data.

References

Arvidson, R.E., Seelos IV, F.P., Deal, K.S., Koeppen, W.C., Snider, N.O., Kieniewicz, J.M., Hynek, B.M., Mellon, M.T., Garvin, J.B., 2003. Mantled and exhumed terrains in Terra Meridiani, Mars. J. Geophys. Res. 108 (E10), doi:10.1029/2002JE001982. 8073.

Bandfield, J.L., Christensen, P.R., Smith, M.D., 2000. Spectral data set factor analysis and end-member recovery: Application to analysis of martian atmospheric particulates. J. Geophys. Res. 105 (E4), 9573–9587.

Bandfield, J.L., Edgett, K.S., Christensen, P.R., 2002. Spectroscopic study of the Moses Lake dune field, Washington: Determination of compositional distributions and source lithologies. J. Geophys. Res. 107 (E11), doi:10.1029/2000JE001469. 5092.

Barron, V., Rendon, J.L., Torrent, J., Serna, C.J., 1984. Relation of infrared, crystallochemical, an morphological properties of Al-substituted hematites. Clays Clay Miner. 32, 475–479.

Bell III, J.F., and 39 colleagues, 2004. Pancam multispectral imaging results from the Opportunity Rover at Meridiani Planum. Science 306, 1703–1708.

Bhagavantam, S., Venkatarayuku, T., 1939. Raman effect in relation to crystal structure. Proc. Indian Acad. Sci. A 9, 224–258.

Born, M., Wolf, E., 1980. Principles of Optics, sixth ed. Pergamon, Tarrytown, NY, pp. 627–633.

Burt, D.M., Knauth, L.P., Wohletz, K.H., 2005. Origin of layered rocks, salts, and spherules at the Opportunity landing site on Mars: No flowing or standing water evident or required. Lunar Planet. Sci. XXXVI. Abstract 1527 [CD-ROM].

Catling, D.C., Moore, J.M., 2003. The nature of coarse-grained crystalline hematite and its implications for the early environment of Mars. Icarus 165, 277–300.

Chan, M.A., Beitler, B., Parry, W.T., Ormo, J., Komatsu, G., 2004. A possible terrestrial analogue for haematite concretions on Mars. Nature 429, 731–734.

Chapman, M.G., 2005. Newly discovered Meteor Crater metallic impact spherules: Report and implications. Lunar Planet. Sci. XXXVI. Abstract 1907 [CD-ROM].

Chapman, M.G., Tanaka, K.L., 2002. Related magma–ice interactions: Possible origins of chasmata, chaos, and surface materials in Xanthe, Margaritifer, and Meridiani Terrae, Mars. Icarus 155, 324–339.

Christensen, P.R., Harrison, S.T., 1993. Thermal infrared emission spectroscopy of natural surfaces: Application to desert varnish coatings on rocks. J. Geophys. Res. 98, 19819–19834.

Christensen, P.R., Ruff, S.W., 2004. The formation of the hematite-bearing unit in Meridiani Planum: Evidence for deposition in standing water. J. Geophys. Res. 109, doi:10.1029/2003JE002233. E08003.

Christensen, P.R., and 15 colleagues, 2000. Detection of crystalline hematite mineralization on Mars by the Thermal Emission Spectrometer: Evidence for near-surface water. J. Geophys. Res. 105, 9623–9642.

Christensen, P.R., Morris, R.V., Lane, M.D., Bandfield, J.L., Malin, M.C., 2001a. Global mapping of martian hematite deposits: Remnants of water-driven processes on early Mars. J. Geophys. Res. 106 (E10), 23873–23886.

Christensen, P.R., and 25 colleagues, 2001b. Mars Global Surveyor Thermal Emission Spectrometer experiment: Investigation description and surface science results. J. Geophys. Res. 106 (E10), 23823–23872.

Christensen, P.R., and 19 colleagues, 2003. Miniature Thermal Emission Spectrometer for the Mars Exploration Rovers. J. Geophys. Res. 108 (E12), doi:10.1029/2003JE002117. 8064.

Conel, J.E., 1969. Infrared emissivities of silicates: Experimental results and a cloudy atmosphere model of spectral emission from condensed particulate mediums. J. Geophys. Res. 74, 1614–1634.

Cowley, E.R., 1969. Symmetry properties of the normal modes of vibration of calcite and α-corundum. Can. J. Phys. 47, 1381–1391.

Estep-Barnes, P.A., 1977. Infrared spectroscopy. In: Zussman, J. (Ed.), Physical Methods in Determinative Mineralogy. Academic Press, London, pp. 529–604.

Glotch, T.D., Morris, R.V., Christensen, P.R., Sharp, T.G., 2004. Effect of precursor mineralogy on the thermal infrared emission spectra of hematite: Application to martian hematite mineralization. J. Geophys. Res. 109 (E7), doi:10.1029/2003JE002224. E7003.

Glotch, T.D., Bandfield, J.L., Christensen, P.R., 2005. Factor analysis and target transformation of mini-TES spectra: Recovery of scene endmembers at Meridiani Planum. Lunar Planet. Sci. XXXVI. Abstract 2174 [CD-ROM].

Hapke, B., 1981. Bidirectional reflectance spectroscopy. 1. Theory. J. Geophys. Res. 86, 3039–3054.

Hapke, B., 1984. Bidirectional reflectance spectroscopy. 3. Correction for macroscopic roughness. Icarus 59, 41–59.

Hapke, B., 1986. Bidirectional reflectance spectroscopy. 4. The extinction coefficient and the opposition effect. Icarus 67, 264–280.

Hapke, B., 1993. Combined theory of reflectance and emittance spectroscopy. In: Pieters, C.M., Englert, P.A. (Eds.), Remote Geochemical Analysis: Elemental and Mineralogical Composition. Cambridge Univ. Press, New York, pp. 31–41.

Herkenhoff, K.E., and 32 colleagues, 2004. Evidence from Opportunity's Microscopic Imager for water on Meridiani Planum. Science 306, 1727–1730.

Hunt, G.R., Vincent, R.K., 1968. Behavior of spectral features in infrared emission from particulate surfaces of various grain sizes. J. Geophys. Res. 73, 6039–6046.

Hynek, B.M., 2004. Implications for hydrologic processes on Mars from extensive bedrock outcrops throughout Terra Meridiani. Nature 431, 156–159.

Hynek, B.M., Arvidson, R.E., Phillips, R.J., 2002. Geologic setting and origin of Terra Meridiani hematite deposit on Mars. J. Geophys. Res. 107 (E10), doi:10.1029/2002JE001891. 5088.

Kirkland, L.E., Herr, K.C., Adams, P.M., 2004. A different perspective for the Mars rover "Opportunity" site: Fine-grained, consolidated hematite and hematite coatings. Geophys. Res. Lett. 31, doi:10.1029/2003GL019284. L05704.

Knauth, L.P., Burt, D.M., Wohletz, K.H., 2005. Impact origin of sediments at the Opportunity landing site on Mars. Nature 438, 1123–1128.

Lane, M.D., 1999. Mid-infrared optical constants of calcite and their relationship to particle size effects in thermal emission spectra of granular calcite. J. Geophys. Res. 104, 14099–14108.

Lane, M.D., Morris, R.V., Mertzman, S.A., Christensen, P.R., 2002. Evidence for platy hematite grains in Sinus Meridiani, Mars. J. Geophys. Res. 107 (E12), doi:10.1029/2001JE001832. 5126.

Lorentz, H.A., 1880. Über die Beziehung zwischen der Fortpflanzungsgeschwindigkeit des Lichtes und der Körperdichte. Ann. Phys. 9, 641–665.

Lorenz, L., 1881. Über die Refractionsconstante. Ann. Phys. 11, 70–103.

Malinowski, E.R., 1991. Factor Analysis in Chemistry, second ed. Wiley, New York.

McLennan, S.M., and 31 colleagues, 2005. Provenance and diagenesis of the evaporate-bearing Burns formation, Meridiani Planum, Mars. Earth Planet. Sci. Lett. 240, 95–121.

Moersch, J.E., Christensen, P.R., 1994. Thermal emission from particulate surfaces: A comparison of scattering models with measured spectra. J. Geophys. Res. 100 (E4), 7465–7477.

Noreen, E., Tanaka, K.L., Chapman, M.G., 2000. Examination of igneous alternatives to martian hematite using terrestrial analogs. Geol. Soc. Am. 32. Abstract A303.

Onari, S., Arai, T., Kudo, K., 1977. Infrared lattice vibrations and dielectric dispersion in α-Fe_2O_3. Phys. Rev. B 16, 1717–1721.

Ormö, J., Komatsu, G., Chan, M.A., Beitler, B., Parry, W.T., 2004. Geological features indicative of processes related to the hematite formation in Meridiani Planum and Aram Chaos, Mars: A comparison with diagenetic hematite deposits in southern Utah, USA. Icarus 171, 295–316.

Pecharromán, C., Iglesias, J.E., 2000. Effect of particle shape on the IR reflectance spectra of pressed powders of anisotropic materials. Appl. Spectrosc. 54, 634–638.

Rendon, J.L., Serna, C.J., 1981. IR spectra of powder hematite: Effects of particle size and shape. Clay Miner. 16, 375–381.

Ruff, S.W., Christensen, P.R., Barbera, P.W., Anderson, D.L., 1997. Quantitative thermal emission spectroscopy of minerals: A laboratory technique for measurement and calibration. J. Geophys. Res. 102, 14899–14913.

Spitzer, W.G., Kleinman, D.A., 1961. Infrared lattice bands of quartz. Phys. Rev. 121, 1324–1335.

Squyers, S.W., and 18 colleagues, 2004. In situ evidence for an ancient aqueous environment at Meridiani Planum, Mars. Science 306, 1709–1713.

Vincent, R.K., Hunt, G.R., 1968. Infrared reflectance from mat surfaces. Appl. Opt. 7, 53–58.

Wenrich, M.L., Christensen, P.R., 1996. Optical constants of minerals derived from emission spectroscopy: Application to quartz. J. Geophys. Res. 101, 15921–15931.